Chum *et al. Earth, Planets and Space* (2016) 68:56
DOI 10.1186/s40623-016-0433-1

Earth, Planets and Space

FULL PAPER

Open Access

Spread F occurrence and drift under the crest of the equatorial ionization anomaly from continuous Doppler sounding and FORMOSAT-3/COSMIC scintillation data

Jaroslav Chum[1*], Jann-Yenq Liu[2], Shih-Ping Chen[2], Miguel Angel Cabrera[3], Jan Laštovička[1], Jiří Baše[1], Dalia Burešová[1], Jiří Fišer[1], František Hruška[1] and Rodolfo Ezquer[4,5]

Abstract

A relatively new method based on measurements by multipoint continuous Doppler sounding is applied to study the occurrence rate, propagation velocities, and directions of spread F structures over Tucumán, Northern Argentina, and Taiwan, both of which were under the crest of the equatorial ionization anomaly in 2014. In addition, spread F is studied globally over the same time period from the S4 scintillation index measured onboard FORMOSAT-3/COSMIC (F3/C) satellite. It is shown that the continuous Doppler sounding gives results that are consistent with S4 data and with previous optical, global positioning system (GPS), and satellite measurements. Most of the spread F events were observed from September to March, i.e., during the local summer half of the year in Tucumán, whereas in Taiwan, the highest occurrence rate was observed around equinoxes. The occurrence rate in Tucumán was about four times higher than that in Taiwan. The propagation velocities and directions were estimated from the Doppler shift spectrograms. The spread structures related to spread F propagated roughly eastward at velocities from ~70 to ~200 m s^{-1} during nighttime hours. The mean observed horizontal velocity was 140 m s^{-1} over Tucumán and 107 m s^{-1} over Taiwan. The local times at which the highest velocities were observed roughly correspond to local times with highest values of scintillation index S4, at ~20 to 23 LT. In addition, a comparison of measured drift velocities with neutral wind velocities predicted by models is provided. The observed velocities usually exceeded the horizontal neutral wind velocities predicted by the HWM14 model for the locations and times of observations.

Keywords: Ionospheric irregularities, Equatorial spread F, Plasma bubbles, Equatorial ionization anomaly, Remote sensing, Doppler sounding, GPS signal occultation and scintillation

Background

Ionospheric irregularities known as spread F often prevent accurate scaling of ionograms and obtaining reliable values of F2 layer peak characteristics such as critical frequency *foF2* and peak height *hmF2* (McNamara et al. 2008), which limits our knowledge of the ionosphere and predictability of conditions for radio wave propagation. Moreover, equatorial and low-latitude spread F is often associated with plasma bubbles and scintillations of global positioning system (GPS) signals (Chen et al. 2006; Shi et al. 2011; Alfonsi et al. 2013), which may cause inaccuracies in position determination. It is generally accepted that equatorial spread F (ESF) and plasma bubbles result from Rayleigh–Taylor instability triggered during the uplift of the F layer owing to the prereversal enhancement of the eastward (zonal) electric field and development of the steep plasma density gradient as the bottomside ionosphere becomes depleted after sunset (Fejer et al. 1999; Stolle et al. 2006; Abdu et al. 2009a; Kelley 2009). The day-to-day variability and the

*Correspondence: jachu@ufa.cas.cz
[1] Institute of Atmospheric Physics, Bocni II/1401, 14131 Prague 4, Czech Republic
Full list of author information is available at the end of the article

roles of all factors that contribute to plasma bubble formation and spread F observation such as gravity wave (GW) seeding, neutral winds, angle between magnetic meridian, and solar terminator, however, remain enigmatic and are subjects of intense investigation (Kudeki et al. 2007; Abdu et al. 2009a, b; Cabrera et al. 2010; Hysell et al. 2014). The prereversal enhancement of the eastward electric field and hence the enhancement of the plasma vertical drift vary with longitude and season and are likely an important controlling factor for large-amplitude equatorial plasma bubble development (Huang and Hairston 2015). 30 MHz coherent backscatter radar observations at Saõ Luís have shown that evening mean upward vertical drifts are a necessary but not sufficient condition for the occurrence of topside ESF echoes (Smith et al. 2015). It is assumed that plasma bubbles are generated above the geomagnetic equator and stretch along the magnetic field lines to low latitudes (Sultan 1996; Keskinen et al. 1998; Bhattacharyya and Burke 2000). The eastward movement of the developed plasma structures at velocities usually exceeding 100 m s^{-1} has been experimentally confirmed by several independent studies (Terra et al. 2004; Haase et al. 2011; Chum et al. 2014). The zonal velocities derived from observations of ionospheric irregularities at night are also eastward with magnitudes decreasing from the geomagnetic equator to the equatorial ionization anomaly (EIA) crests (Kil et al. 2002). The mean zonal velocities of ionospheric irregularities at the Brazilian Saõ Luís equatorial station were larger during the December solstice and decayed during the equinoctial periods (Muella et al. 2009). Low-latitude all-sky imager observations in northern Argentina and Peru revealed at stations closer to the magnetic equator weaker (stronger) eastward plasma drifts in the postsunset (postmidnight) period (Martinis et al. 2003). Incoherent scatter radar observations at Jicamarca (Fejer et al. 2005) indicate daytime westward drifts and stronger nighttime eastward drifts under quiet conditions; nighttime perturbation drifts increase strongly with solar activity. Pacheco et al. (2011) investigated local-time variations of zonal drifts at different latitudes, longitudes, and seasons using data from the Republic of China Satellite-1 (ROCSAT-1). Superrotation of the ionosphere was observed in zonal drift measurements, particularly at lower latitudes.

ESF has been studied by ground-based measurements using optical airglow cameras, radars, ionosondes, and GPS receivers (Haase et al. 2011; Fejer et al. 1999; Shi et al. 2011) and in situ measurements using satellite observations. Either direct in situ measurements of plasma density depletions (Huang et al. 2001; Park et al. 2005) or their magnetic signatures owing to the diamagnetic effect of plasma can be used to study the properties and distributions of plasma bubbles by satellites (Luhr et al. 2003; Stolle et al. 2006).

In this paper, we present horizontal velocities of spread F structures observed by multipoint continuous Doppler sounding over Tucumán, Northern Argentina (27°S, 65°W, inclination of magnetic field $I = 27°$), and over Taiwan (24°N, 121°E, inclination of magnetic field $I = 35°$) and we compare the values with neutral wind velocities obtained from recent experimental model HWM14 (Drob et al. 2015). The occurrence rates of spread F structures observed by Doppler sounding are compared with the new data from global radio occultation measurements of GPS signal scintillation onboard the FORMOSAT-3/COSMIC (F3/C) satellites. Both regions of Doppler sounding are located under the crest of the EIA; Tucumán is under the southern crest, whereas Taiwan is under the northern crest. The time shift between these regions is about 12 h. Although continuous Doppler sounding was used to investigate wave-like disturbances in the ionosphere in the 1960s (Davies et al. 1962; Davies and Baker 1966), its application to ESF studies is relatively new and rare. To the best of our knowledge, Chum et al. (2014) were the first to use Doppler shift measurements for spread F investigations. They presented systematic analysis of propagation velocities of spread F structures based on multipoint continuous Doppler sounding over Tucumán from December 2012 to November 2013. Their results can be summarized as follows. Spread F occurred at night generally in the local summer half of the year and propagated roughly eastward at typical velocities of ~100–160 m s^{-1}. This result is consistent with those other reports based on airglow, ionosonde, and GPS measurements (Terra et al. 2004; Haase et al. 2011; Alfonsi et al. 2013). The advantage of continuous Doppler sounding compared with optical measurements is its independence of tropospheric weather conditions. The Doppler shift spectrograms provide a relatively simple and rapid qualitative overview of the spread F occurrence; however, its relatively low accuracy of velocity determination is a disadvantage.

The Doppler shift measurements have relatively high time resolution of ~10 s and complement the ionosonde measurements. These measurements can be used among others for the monitoring of spread F, which is a severe limitation for radio propagation at low latitudes. This paper builds on the previous work and methods described by Chum et al. (2014), and its motivation is as follows. The continuous Doppler sounder measurement data were previous applied to investigations of ESF only once for one station (Tucumán) using one year of data (Chum et al. 2014). In the present study, we use two stations, Tucumán under the southern crest of EIA near the South Atlantic magnetic anomaly (Hartmann

and Pacca 2009) and Taiwan under the northern crest of EIA in southeastern Asia, to obtain statistical information on ESF behavior at two significantly different locations, and we add one more year of data. In addition, the spread F occurrence and its global distribution are studied from F3/C satellite data, particularly from the occultation measurements of the GPS signal scintillation. This investigation is similar to a local study of spread F and scintillations over Sanya by Zhang et al. (2015), who showed that spread F and large scintillations occur simultaneously. As the second objective, we verify that the new method of spread F velocity measurements based on continuous Doppler sounding gives values consistent with previously published results based on different methods of measurement and that these values properly describe the reported longitudinal differences. In the past, this was only partly achieved for one station (Tucumán). In the present study, spread F occurrences and velocities are additionally studied over Taiwan and Tucumán in 2014, where the multipoint continuous Doppler sounding systems (CDSSs) have been installed, primarily to examine the wave activity in the low-latitude ionosphere. (The Doppler sounder installed in Taiwan in late 2013 has provided reliable data only since 2014.) Details on velocity distributions and occurrence rates of spread F structures in these locations are provided in "Occurrences and velocities over Taiwan and Tucumán and global distribution of spread F from S4 measurements by F3/C" section, and a comparison with previous reports is given in the first part of "Comparison with other measurements and relation to neutral winds from HWM14 model" section. The third goal of the current work is comparison of spread F velocities with neutral winds obtained from the recent neutral wind model HWM14 (Drob et al. 2015). This comparison is motivated by the theoretical prediction that the plasma drifts in the nighttime equatorial F2 region should approach neutral wind velocities (Kelley 2009). The measurements of spread F/plasma depletion drift velocities thus can serve as additional information in the evaluation of empirical wind models at these locations. This comparison is partly inspired by the work of England and Immel (2012), who reported that the previous HWM07 model shows discrepancies with drift velocities of equatorial and low-latitude plasma depletions observed by the far ultraviolet imager on the IMAGE spacecraft.

Measurements and data analysis

Continuous Doppler sounding considers that the sounding radio wave experiences frequency shift, known as Doppler shift, if the ionospheric layer from which the wave reflects moves or if processes occur that lead to plasma compression or rarefaction (Davies et al. 1962; Chum et al. 2012, and references therein). The CDSS, used in both Tucumán and Taiwan, consists of three transmitters known as Tx1, Tx2, and Tx3 that form a roughly equilateral triangle with sides of about 100 km. The sounding frequencies of the transmitters are mutually shifted by ~4 Hz at the specific region so that all of the sounding paths corresponding to different transmitter–receiver pairs can be easily displayed in one Doppler shift spectrogram. The geographical coordinates of the system installed in Tucumán have been presented in Fig. 2 in Chum et al. (2014) and include transmitters Tx1 (26.943°S, 65.707°W), Tx2 (26.563°S, 64.550° W), Tx3 (27.499°S, 64.874°W), and receiver Rx (26.840°S, 65.230°W). The coordinates of the system deployed in Taiwan are Tx1 (23.897°N, 121.551°E), Tx2 (24.341°N. 120.778°E), Tx3 (24.816° N, 121.727°E), Rx0 (24.972°N, 121.192°E), and Rx1 (23.955°N, 120.927°E). The transmitted power was only ~1 W, and the sounding frequencies were 4.63 MHz in Tucumán and 6.57 MHz in Taiwan. The reflection heights were determined from nearby ionospheric sounders.

Figures 1 and 2 show examples of Doppler shift spectrograms recorded in Tucumán and Taiwan, respectively. The colors indicate the received power spectral densities in arbitrary units; the antennas were not calibrated. Figure 1 presents a more complicated record because several oblique spread structures (OSSs) were observed during the displayed time interval, whereas only one OSS occurred on each signal path in Fig. 2. The observation of several OSSs during one night occurred more frequently than that of a single event in both Tucumán and Taiwan. The remarkable undulations (short-period waves) that preceded the first OSS in Fig. 1 were relatively rare for both locations and were observed only in about 10 % of the events. Both examples were recorded on geomagnetically quiet days on February 2 and March 16, 2014, when the Kp fluctuated around 1 and was less than one, respectively.

Figure 3 shows ionograms recorded in Tucumán at the time period in which the OSSs presented in Fig. 1 were recorded. A spread F, which could be categorized as strong-range spread F (Shi et al. 2011; Alfonsi et al. 2013), was observed at 01:10 UT (Fig. 3b) and at 02:40 UT (Fig. 3d), which are the times in which the OSSs were observed in the Doppler shift spectrogram in Fig. 1. On the contrary, the spread F was not measured before and between the occurrence of the individual OSSs at 00:30 UT (Fig. 3a) and 01:50 UT (Fig. 3c), respectively. Another example of simultaneous occurrence of OSSs and spread F over Tucumán was given by Chum et al. (2014). An example of simultaneous occurrence of OSS and spread F in Taiwan is given in Fig. 4, which shows a sequence of ionograms recorded at 14:20, 14:40, 15:00, and 15:20

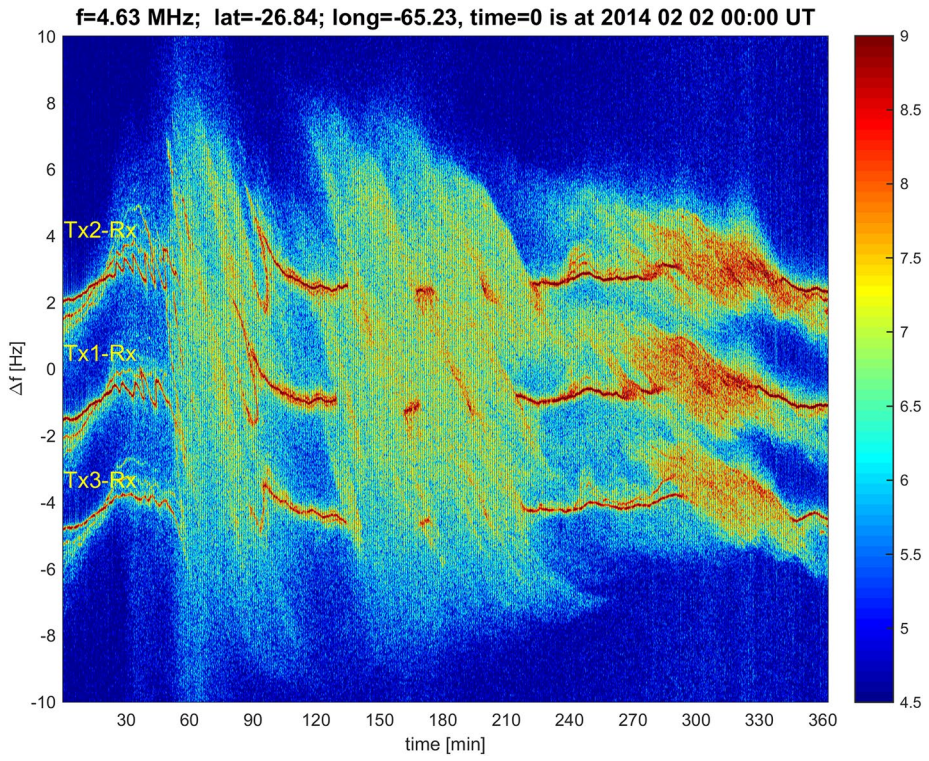

Fig. 1 Doppler shift spectrogram computed from data recorded in Tucumán on February 2, 2014, from 00:00 UT to 06:00 UT (solar local time LT = UT − 4.3)

UT on March 16, 2014. The distinct spread F measured at 14:40 (Fig. 4b) and 15:00 UT (Fig. 4c) corresponds to the OSS occurrence in Fig. 2.

We also examined whether large scintillations are recorded during the OSS events. Figure 5 shows the scintillation index S4, defined as standard deviation normalized to the mean value during 1-min intervals, for PRN3 (red) and PRN19 (blue) satellites recorded in Tucumán from 0:00 to 4:00 UT on February 2, 2014. The satellites passed roughly from zenith to the north during this time interval (PRN3 ahead of PRN19). The PRN3 was set below the horizon at approximately 3:15 UT (195 min). Very distinct scintillations were observed at the times of the OSSs occurrences with smaller scintillations from ~90 to 130 min (01:30–02:10 UT), which is consistent with the gap between OSSs occurrence (Fig. 1) at that time. The extremely large values of S4 index from ~140 to 200 min are likely associated with low satellite elevation angles and signal paths that are quasi-parallel with irregularities, which are expected to extend along the magnetic field lines (e.g., Bhattacharyya and Burke 2000; Haase et al. 2011). A statistical comparison of OSS occurrences with S4 index based on radio occultation measurements of GPS signal scintillation onboard the F3/C satellites is provided in "Occurrences and velocities over Taiwan and Tucumán and global distribution of spread F from S4 measurements by F3/C" section.

It is also interesting to examine the ionograms measured close to the geomagnetic equator from which the irregularities are expected to originate (Sultan 1996; Bhattacharyya and Burke 2000). Figure 6 shows a sequence of ionograms recorded in Jicamarca (12°S, 76.8°W), which is the closest equatorial ionosonde to Tucumán. The point at the geomagnetic equator magnetically conjugated with Tucumán is 10.5°S, 67.4°W; Jicamarca is about 1000 km from this point. The mean height of equatorial points conjugated with the altitudes of OSS observations in Tucumán is ~760 km. The individual ionograms in Fig. 6 were measured at the same times as the ionograms in Tucumán in Fig. 3. The strong spread F began at about the same time in Jicamarca and Tucumán on that particular night; however, the spread F continued much longer in Jicamarca, approximately to 7:00 UT, and the lowest values were recorded between ~3:10 and ~3:40. In general, the examination of other days showed that the precise timing, including the beginning, differed among cases and that the spread F was usually observed longer in closer proximity to the geomagnetic equator. Figure 7 shows a sequence of ionograms recorded in Sanya (18.3°N, 109.6°E), which is the

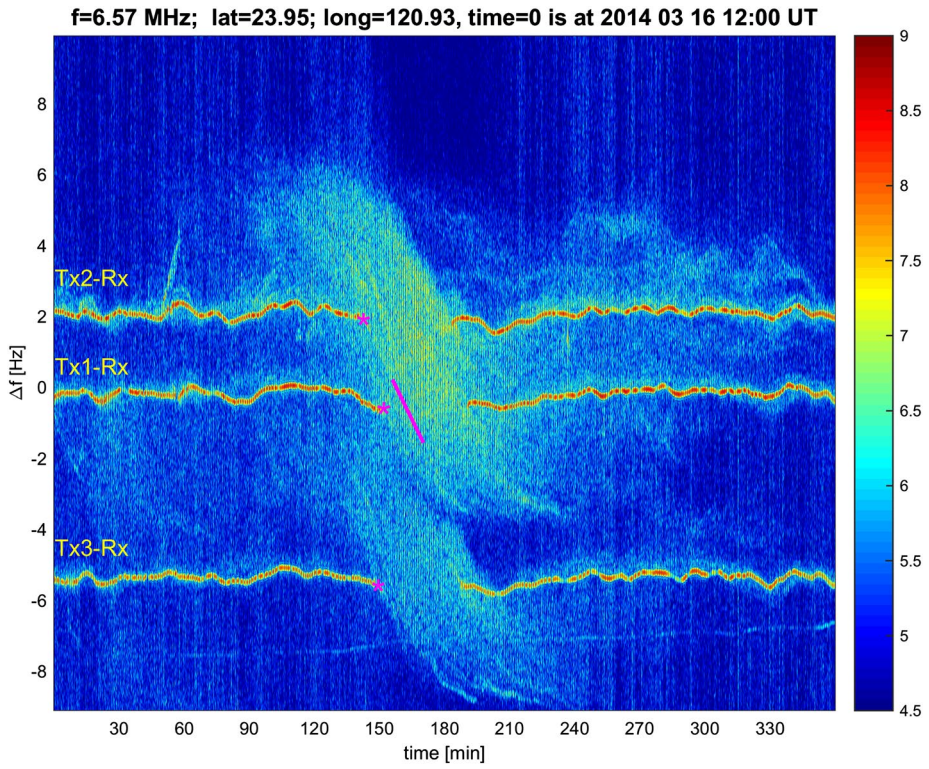

Fig. 2 Doppler shift spectrogram computed from data recorded in Taiwan by the receiver Rx1 on March 16, 2014, from 12:00 UT to 18:00 UT (solar local time LT = UT + 8.1). *Magenta asterisks* show the determined times of OSS beginning; *magenta line* represents the evaluated tilt $\Delta f_D/\Delta T$

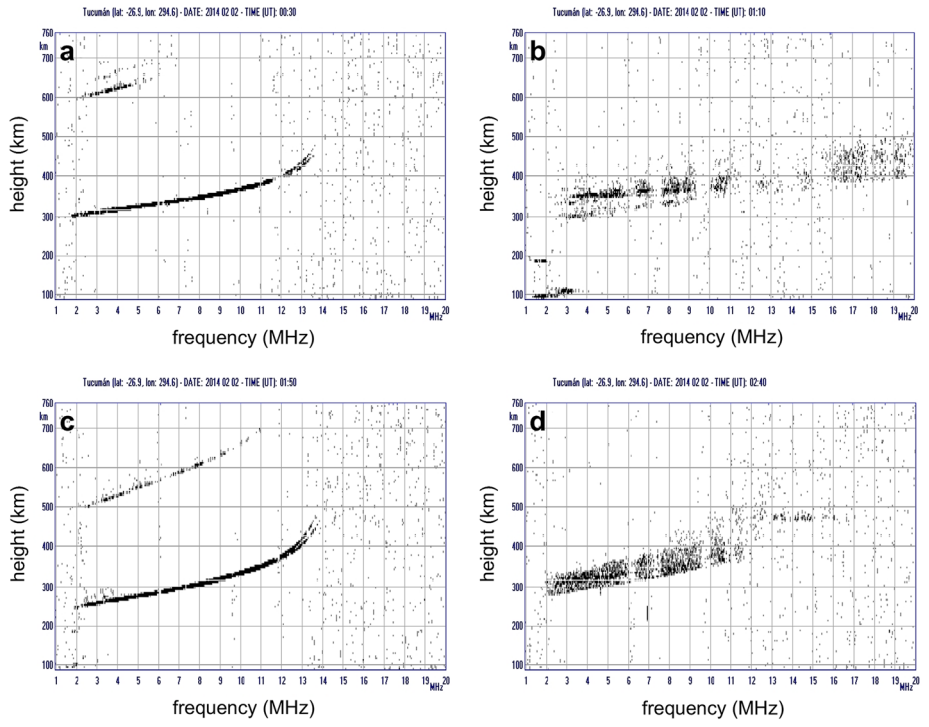

Fig. 3 Sequence of ionograms measured in Tucumán (26.9°S, 65.4°W) at **a** 00:30, **b** 01:10, **c** 01:50, and **d** 02:40 UT (solar local time LT = UT − 4.3) on February 2, 2014

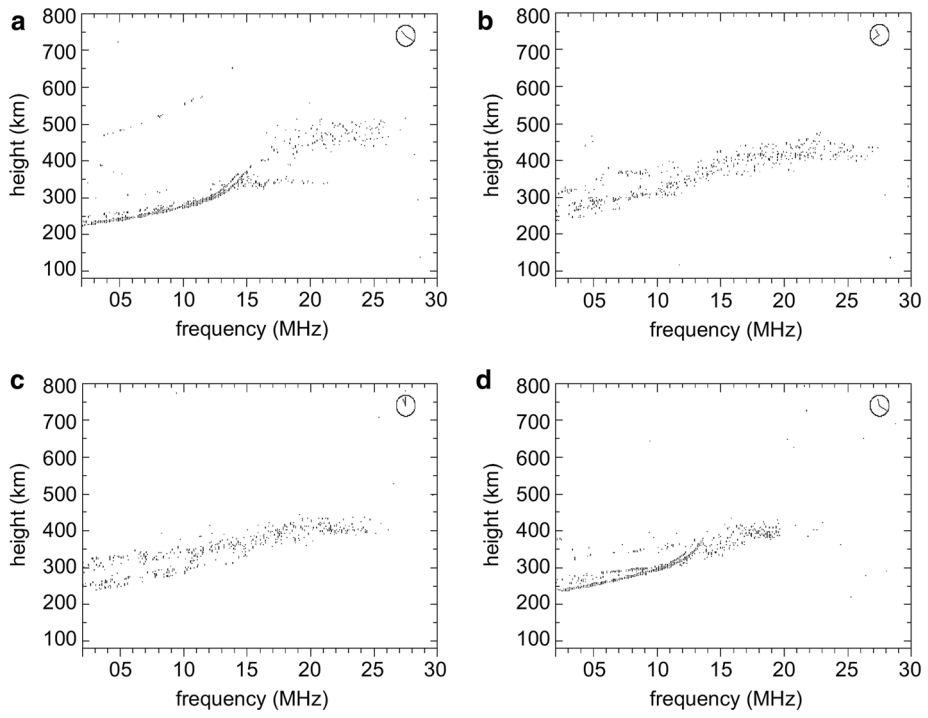

Fig. 4 Sequence of ionograms measured in Zhongli, Taiwan (25.0°N, 121.2°E) at **a** 14:20, **b** 14:40, **c** 15:00, and **d** 15:20 UT (solar local time LT = UT + 8.1) on March 16, 2014

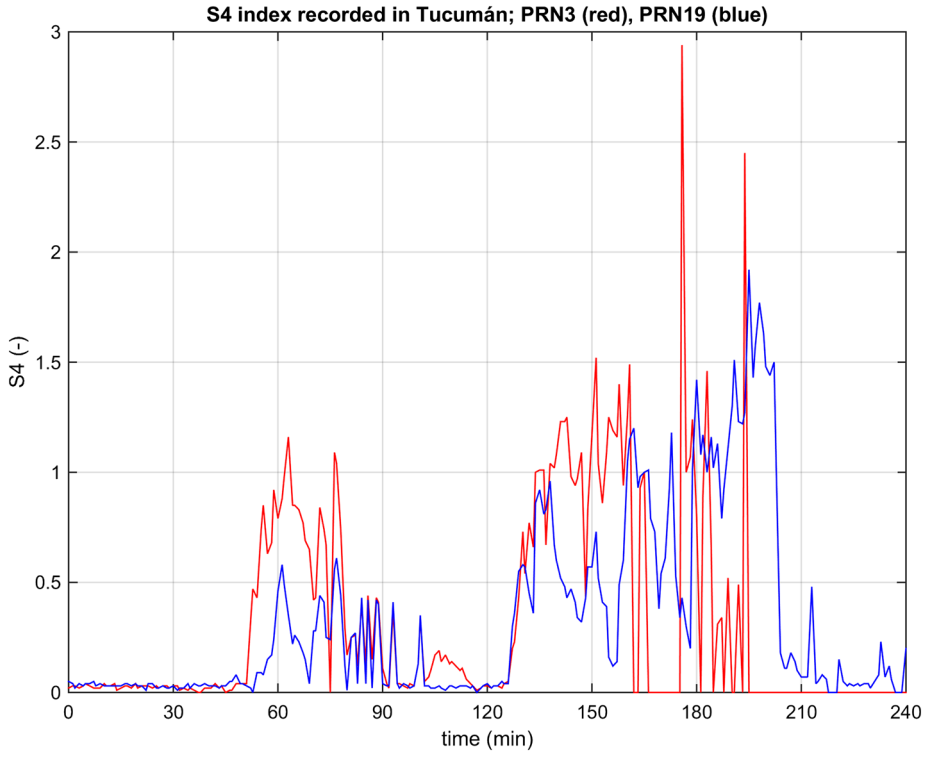

Fig. 5 Scintillation index S4 for signals from PRN3 (*red*) and PRN19 (*blue*) GPS satellites measured in Tucumán from 00:00 to 04:00 UT on February 2, 2014

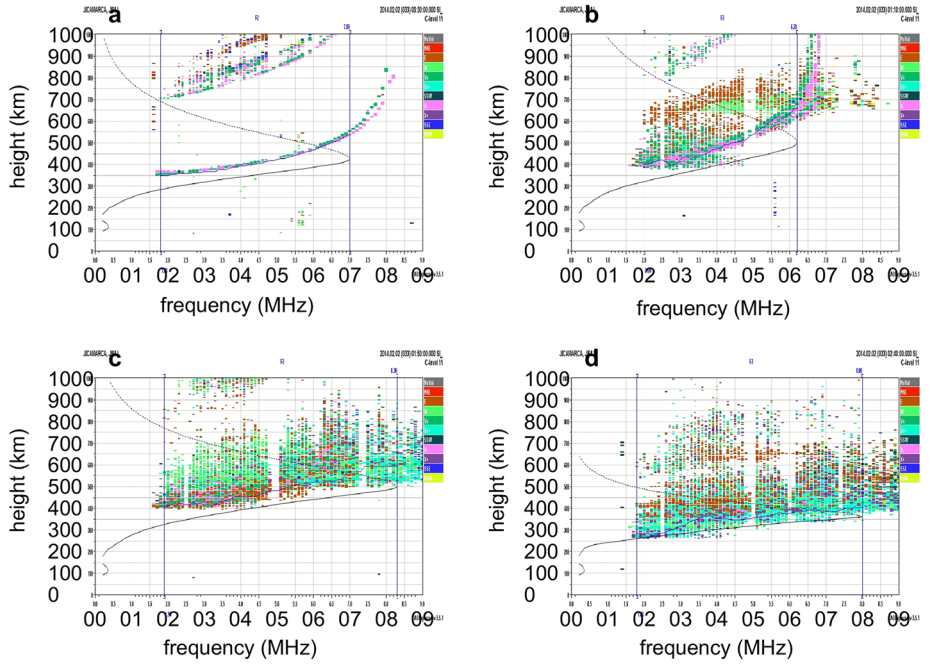

Fig. 6 Sequence of ionograms measured in Jicamarca (12°S, 76.8°W) at **a** 00:30, **b** 01:10, **c** 01:50, and **d** 02:40 UT on February 2, 2014

closest available near-equatorial ionosonde to Taiwan. The point at the geomagnetic equator magnetically conjugated with Taiwan is (7.7°N, 121.6°E); Sanya is about 1700 km from this point. The mean height of equatorial points conjugated with the altitudes of OSS observations in Taiwan is ~940 km. The individual ionograms were recorded at similar times as the ionograms in Taiwan in Fig. 4; the sounding of the ionosondes was not synchronized. The sequence of ionograms in Fig. 7 documents that spread F had longer duration in Sanya, closer to the equator, than in Taiwan. The spread F in Sanya began earlier in this case.

Another point worth mentioning is that the OSSs were observed with time delays between different sounding paths. These time delays, together with known separations of the transmitters, can be used to estimate the propagation velocities and directions of OSSs. More precisely, the separations of reflection points, which are assumed to be the midway between the individual transmitters and receiver, were used in these calculations. It is necessary to stress that it was not possible to determine the time delays reliably for a number of OSS events, e.g., we were not able to determine the time delays for the first OSS event in Fig. 1 observed from ~01:00 to 01:30 UT. The time delays are usually measured as time differences between the beginnings of the OSSs recorded on different sounding paths. The determination of these beginnings is performed manually by clicking in the Doppler shift spectrogram in MATLAB software; an example of the determined OSS beginning times is represented by magenta asterisks in Fig. 2. It is therefore partly subjective, and the estimated average error of the time determination is 1 min. This error propagates into the error estimates, or uncertainties, of the calculated velocities and azimuths.

Chum et al. (2014) reported that it is possible to estimate the horizontal propagation velocities of OSSs, but not their directions, by using another independent method that gives results consistent with calculations based on the time delays. They showed that the horizontal velocity v_H can be calculated as

$$v_H = \sqrt{\frac{\Delta f_D}{\Delta T}\frac{h_0 c}{2f_0}}, \tag{1}$$

$$\Delta f_D = f_D(t_1) - f_D(t_2),$$
$$\Delta T = t_2 - t_1,$$

where $f_D(t_1)$ and $f_D(t_2)$ are Doppler shifts at times t_1 and t_2, respectively; h_0 is the height of the reflecting level; c is the speed of light; and f_0 is the sounding frequency. Equation (1) is derived from the fact that the Doppler shifts for a specific point of reflection—a horizontally moving small-scale irregularity—are $f_D(t_{1,2}) = 2f_0 v_H \sin(\delta_{1,2})/c$, where angles δ_1 and δ_2 are deviations from the vertical for the positions at times t_1, t_2. During the

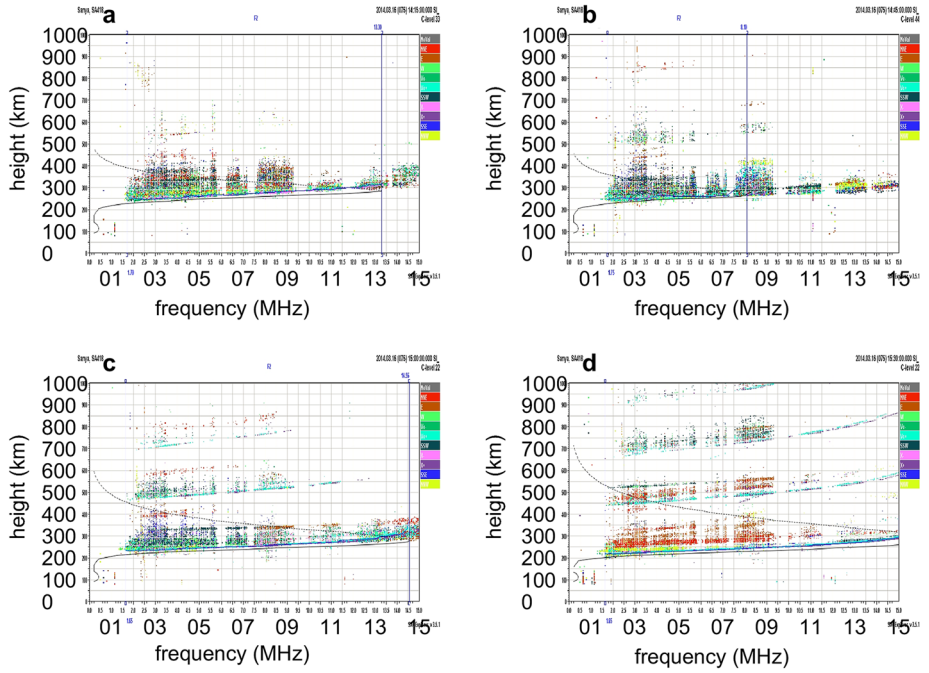

Fig. 7 Sequence of ionograms measured in Sanya (18.3°N, 109.6°W) at **a** 14:15, **b** 14:45, **c** 15:00, and **d** 15:30 UT on March 16, 2014

interval ΔT, the irregularity travels a horizontal distance of $v_H \Delta T = h_0(\tan\delta_1 - \tan\delta_2)$ if we include the sign of the angles. Obviously, Eq. (1) is valid only for small angles δ_1 and δ_2, for which $\sin(\delta_1) \approx \tan(\delta_1) \approx \delta_1$ and $\sin(\delta_2) \approx \tan(\delta_2) \approx \delta_2$. That is, measurement of the tilt $\Delta f_D/\Delta T$ should be performed only in the linear part of the OSS in which the tilt remains constant, $df_D/dt = \text{const}$.

There are two main sources of uncertainties in the application of Eq. (1). First, as follows from the nature of spread F, the reflection height is of a random character, and the signal reflects from many different small-scale irregularities. It is difficult to determine the reflection height h_0 during the spread F event; it is generally impossible to be determined from ionograms. We therefore used the IRI 2012 model to estimate the reflection height assuming that the average net uncertainty, or scatter range at ESF conditions plus the inaccuracy of IRI 2012, considering h_0 is 50 km, $\varepsilon_{h0} = 50$ km. This value is approximately one-fifth of the average reflection height, $h_0 = 250$ km. In addition, sometimes it is difficult or partly subjective to measure the tilt of OSSs if they are blurry; an example of the $\Delta f_D/\Delta T$ evaluation is marked in magenta color in Fig. 2. Moreover, the tilts of some OSSs change and are usually smaller when the OSSs end. It is impractical and partly impossible to estimate the uncertainty for each event individually. Therefore, on the basis of our evaluation of Doppler records and comparison with velocities obtained by the time delay method, we determined the average uncertainty in ΔT to be about 3 min, $\varepsilon_{\Delta T} = 3$ min. Fortunately, the horizontal velocity v_H is proportional to square root of both h_0 and $\Delta f_D/\Delta T$; thus, we can still obtain reasonable estimates of v_H despite the relatively large uncertainties of h_0 and $\Delta f_D/\Delta T$. The uncertainty of v_H is calculated by Eq. (2) as the maximum deviation from the value obtained from Eq. (1) assuming the height h_0 and time interval ΔT to be increased and decreased, respectively, by the above discussed uncertainties ε_{h0} and $\varepsilon_{\Delta T}$:

$$\varepsilon(v_H) = \sqrt{\frac{\Delta f_D}{\Delta T - \varepsilon_{\Delta T}} \frac{(h_0 + \varepsilon_{h0})c}{2f_0}} - v_H, \qquad (2)$$

where v_H is calculated from Eq. (1). We took the uncertainty, or deviation, toward the larger values of v_H because it is always larger than that toward the smaller values. It is shown in "Occurrences and velocities over Taiwan and Tucumán and global distribution of spread F from S4 measurements by F3/C" section that the propagation velocities calculated from the time delays between the observations of specific OSSs on different sounding paths (time delay method) are consistent with velocity estimates based on the tilt $\Delta f_D/\Delta T$ measurements (tilt method).

It should also be noted that in the initial phase of development of a geomagnetic field-aligned equatorial plasma bubble, which gives rise to spread F, the bubbles

may have large upward velocities that often exceed the horizontal velocity in magnitude. This upward velocity could substantially affect the Doppler shift and hence the tilt method. However, this initial development is realized at very low latitudes close to the geomagnetic equator, whereas our measurements were located in the EIA crest region sufficiently far from this area, as described in "Background" section. Thus, we can assume that the irregularity movement is predominantly horizontal in the region of our measurements. Therefore, the application of the tilt method for estimating the horizontal velocities of spread F structures is justified. The fact that the horizontal movement is dominant in our observations is also supported by the examples in Figs. 1 and 2. In these figures, the OSSs reach both positive and negative values of Doppler shift in a roughly symmetrical manner with respect to the signals in time intervals in which the spread features were not observed. The potential influence of vertical motion is also partly compensated by the fact that we used differential and not absolute values of Doppler shifts in Eq. (1). It should be noted that a constant offset of Doppler shift should not affect the results of our measurements. However, the tilt method could lead to incorrect results if measurements are conducted close to the geomagnetic equator when instability develops and plasma bubbles are created.

The GPS signal scintillations were obtained from the radio occultation measurements onboard the F3/C satellites. The Constellation Observing System for Meteorology, Ionosphere, and Climate mission (COSMIC) is formed by six microsatellites at 800 km low Earth orbit (LEO) and a 72° orbital inclination angle. The radio GPS occultation experiment (GOX) performs radio occultation observations in both the atmosphere and the ionosphere, and the radio scintillation of the GPS L1 band C/A code (1.575 GHz) is calculated and recorded as the S4-index, which is a standard deviation of the received power normalized by its mean value (http://cdaac-www.cosmic.ucar.edu/cdaac/doc/documents/s4_description.pdf). An average of 2000–3000 occultation scintillation profiles is recorded per day in the scintillation files (data type scnLv1) and can be obtained from Taiwan Analysis Center for COSMIC (TACC) and the COSMIC Data Analysis and Archive Center (CDAAC).

To specify the location and time of the most intensive scintillation, the maximum value $S4_{max}$ on each profile is determined. According to the time, location, and altitude of the observation, each $S4_{max}$ is assigned to its proper grid in a three-dimensional (3D) map. A median value of $S4_{max}$ is then computed in a specific region in the 3D map over a specific time period, which in our case was the year 2014.

Occurrences and velocities over Taiwan and Tucumán and global distribution of spread F from S4 measurements by F3/C

Figure 8 displays the time intervals of occurrences of the OSS events over Tucumán in 2014 as functions of day of year (horizontal axis) and daytime (vertical axis). The horizontal velocities v_H calculated by Eq. (1) are depicted by color. The tilt method was chosen for calculations of v_H because it can be applied to all of the detected OSS events. It should be noted that the tilt method is usable even if one or two transmitters are not operating for reasons such as power supply failure; the same is not true for the time delay method. The horizontal thick black lines indicate data gaps when the receiver was not operating or was malfunctioning. The blue dashed curves show the times of sunset and sunrise on the ground. The results in Fig. 8 confirm the previous findings by Chum et al. (2014) such that the OSSs occur in Tucumán after sunset (at night) mainly from September to March (April) and that they are only exceptionally observed in other months. In total, 314 OSS events that occurred during 115 days were analyzed. However, because the data were missing for more than 93 days, the mean probability over one year that at least one OSS event will be observed during a night was $115/(365 - 93) = 0.42$. For the period September to March, this probability was substantially higher, at almost 0.76, whereas it was only 0.08 for the period April to August. The mean height of reflection for 4.63 MHz waves from the IRI 2012 model at the times of the OSS events was 244 km with a 21-km standard deviation of distribution. The mean observed horizontal velocity of the OSSs was 140 m s^{-1}, and the standard deviation of distribution was 29 m s^{-1}. The mean uncertainty was 40 m s^{-1}.

Figure 9 presents the distribution and velocities of the OSS events over Taiwan in the same manner as those for Tucumán in Fig. 8. The data from the receiver Rx1 were used because frequent short-time data gaps and interference in the receiver Rx0 disturbed the measurements and made the data analysis difficult or impossible. The mean height of reflection for 6.57 MHz waves from the IRI 2012 model at the times of OSS events was 264 km with a 19-km standard deviation of distribution. As expected, the OSSs were observed in Taiwan at night, similar to those in Tucumán. Remarkably, we detected significantly fewer OSS events in Taiwan than in Tucumán; only 59 events were detected during 30 nights in Taiwan. However, the data were missing for more than 104 days. Therefore, the mean probability over 1 year that at least one OSS event will be observed at night was $30/(365 - 104) = 0.11$, which is about four times less than in Tucumán. The second difference is that the OSSs were mostly observed around equinoxes in Taiwan rather than

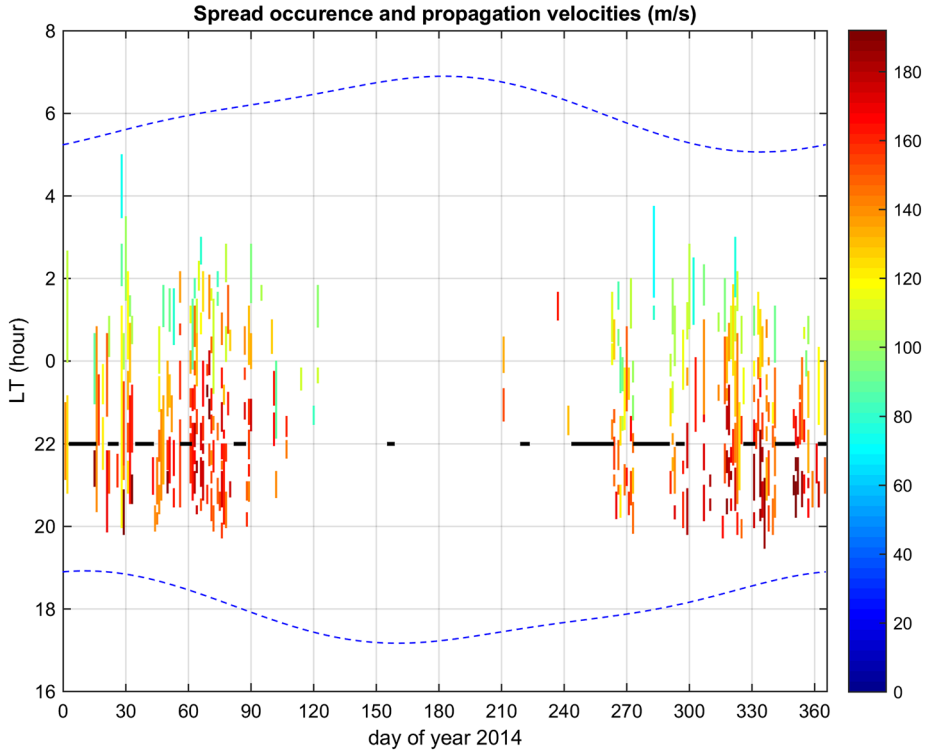

Fig. 8 Spread F occurrence and horizontal velocities in m s^{-1} (*color coded*) as a function of day of year and daytime for Tucumán in 2014 estimated from the tilt $\Delta f_0/\Delta T$. *Horizontal black thick lines* indicate data gaps; *dashed blue curves* show the times of sunset and sunrise at the altitude of 0 km

in the local summer half of the year as in Tucumán. The third difference is the lower mean velocity over 1 year, which was only 107 m s^{-1} with a 17 m s^{-1} standard deviation of distribution; the mean uncertainty was 27 m s^{-1}.

The velocity distributions are displayed in histograms presented in Fig. 10, which shows the occurrence frequencies of OSS velocities with a velocity step of 10 m s^{-1} for Tucumán (top) and Taiwan (bottom). Figure 10 confirms that the number of OSS events was significantly higher in Tucumán than in Taiwan and that the propagation velocities in Tucumán were usually higher than those in Taiwan. It should be noted that the velocity bin of 10 m s^{-1} is lower than the typical estimated uncertainty of propagation velocities.

The top panel in Fig. 11 presents the azimuths of propagation obtained by the time delay method for Taiwan. The OSSs propagated roughly eastward in a relatively narrow range of azimuths; the mean azimuth was 89° with a 15° standard deviation of distribution. In total, 22 events were analyzed by using the time delay method, i.e., about 40 % of all the detected events; the time delay method was not applicable for the remaining events. The bottom panel in Fig. 11 shows the propagation velocities with error bars (bottom plots) calculated by the time delay method (blue) and by the tilt method (magenta) for Taiwan as a function of daytime. It can be verified that both methods gave consistent results within the estimated uncertainties; the mean uncertainty of velocities obtained by the tilt method and by the time delay method was 27 and 12 m s^{-1}, respectively. The results for Tucumán are very similar to those shown by Chum et al. (2014) for 2013. The mean azimuth in Tucumán in 2014 was 88° with an 18° standard deviation of distribution. In total, 143 OSS events from 314 were analyzed in Tucumán by using the time delay method. It should be stressed that all events analyzed by the time delay method were also analyzed by the tilt method in both locations and that the data cover all months of OSS occurrence. The observed velocities were usually lower late at night than after sunset (Figs. 8, 9, 11).

Figure 12a presents the global distribution of $S4_{max}$ for the altitude range of 200–300 km, which is the altitude range of Doppler observations. As expected, the scintillation index reached the highest values around the geomagnetic equator, where the ESF occurs most frequently. The largest index values were observed approximately between longitudes of −10° and −60°. Figure 12c, d displays $S4_{max}$ in the altitude range of 200–300 km as a function of local time and season over Tucumán and Taiwan, respectively. These plots are therefore similar to those in

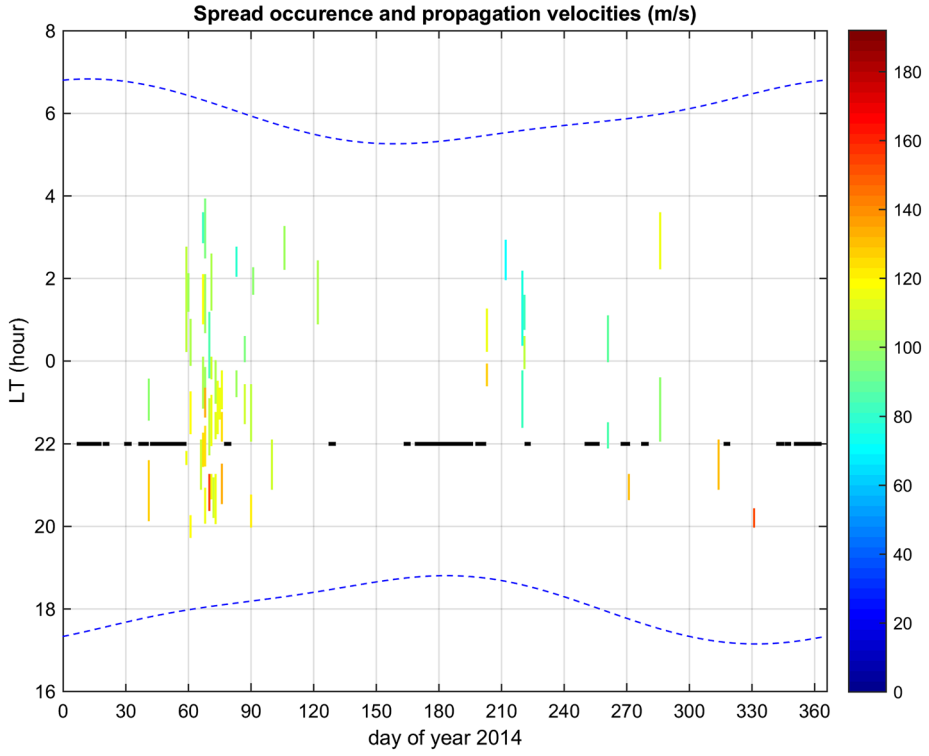

Fig. 9 Spread F occurrence and horizontal velocities in m s^{-1} (*color coded*) as a function of day of year and daytime for Taiwan in 2014 estimated from the tilt $\Delta f_0/\Delta T$. *Horizontal black thick lines* indicate data gaps; *dashed blue curves* show the times of sunset and sunrise at the altitude of 0 km

Figs. 8 and 9 that show the daytime and seasonal distribution of OSSs observed by Doppler. A comparison of Fig. 12c with Fig. 8 and Fig. 12d with Fig. 9 shows that significant $S4_{max}$ values were generally observed at similar times and seasons when most of the OSSs were detected by Doppler. Moreover, the largest values of $S4_{max}$ are observed from ~20:00 to ~23:00 LT, when the highest velocities of OSSs were usually measured. A small peak of $S4_{max}$ values was observed over Taiwan approximately in June at close to 19:00 LT. This peak has no counterpart in Fig. 9; however, we should note that a relatively large gap in Doppler data also occurred on these days. In addition, the June peak in the $S4_{max}$ data might have been caused partly by the sporadic E (Es) layer, as is shown in Fig. 13f.

Figure 13 shows the dependence of $S4_{max}$ on altitude in various forms. Figure 13a, b shows $S4_{max}$ values as a function of local time and altitude for Tucumán and Taiwan, respectively. Figure 13c, d shows the same dependence as Fig. 13a, b but for the locations at the geomagnetic equator, which are magnetically conjugated with Tucumán and Taiwan, respectively. Figure 13e, f presents the $S4_{max}$ values as a function of season and altitude for Tucumán and Taiwan, respectively. It is obvious that the altitude range of ~200–300 km, which is the region of the largest electron densities, dominantly contributes to scintillations. Another peak appearing near ~100 km in Taiwan corresponds to the Es layer. The occurrence of the Es layer was significantly lower in Tucumán. These results are consistent with the study of Arras et al. (2008), who showed that the Es layer occurs relatively rarely over South America likely because of the South Atlantic anomaly.

Another point worth mentioning is that the scintillation reached maximum at about the same local time at the geomagnetic equator and under the crest of the EIA, as shown by comparisons of Fig. 13a, c and b, d. This result could indicate that the spread F and possibly plasma bubbles evolve very quickly along the magnetic field lines as suggested by Bhattacharyya and Burke (2000). However, this statistical study based on $S4_{max}$ indices cannot provide reliable information on the ESF time evolution; dedicated investigations based on detailed case studies and simultaneous multipoint observations are needed verify this reaction.

Comparison with other measurements and relation to neutral winds from HWM14 model

It is interesting to compare the occurrence rates of OSS events with the occurrence rates of plasma bubbles observed by satellites. The fact that OSSs are more

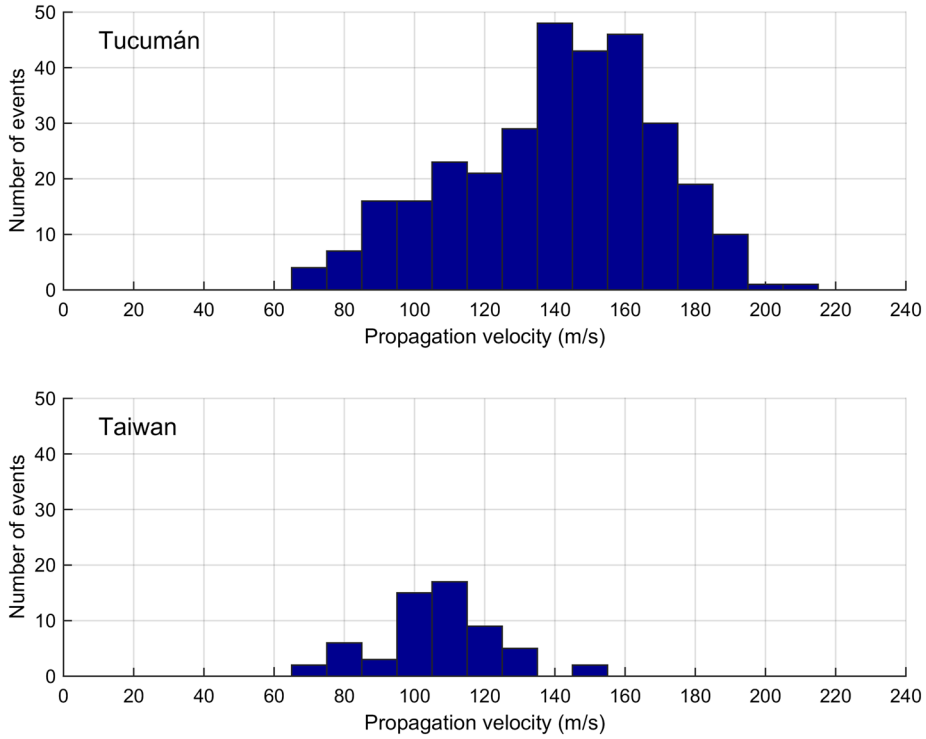

Fig. 10 Histogram of propagation velocities of oblique spread structures (OSSs) for Tucumán (*top*) and Taiwan (*bottom*) determined by the tilt method

frequent in Tucumán than in Taiwan and that they mostly occur from September to March in that region is consistent with the occurrence rates of plasma bubbles as derived from magnetic signatures on the CHAMP satellite orbiting at altitudes of ~450–380 km (Stolle et al. 2006). Similar results were obtained from direct plasma density measurements onboard DMSP F9 and F10 satellites orbiting at ~840 km altitude (Huang et al. 2001) and with recent measurement of prereversal enhancement of ion vertical drift by the C/NOFS satellite (Huang and Hairston 2015). Two factors likely contributing to the higher occurrence rates of OSS events and spread F events in Tucumán than those in Taiwan include a weaker Earth magnetic field in Tucumán, which is close to the South Atlantic magnetic anomaly, and a longitudinal distribution of prereversal enhancements of the equatorial electrojet. The seasonal distribution of OSSs in Tucumán is also consistent with the occurrence of the spread F and scintillation reported for Tucumán (e.g., Alfonsi et al. 2013; Ezquer et al. 2003). For Taiwan, Lee et al. (2013) reported a different seasonal distribution of spread F. On the basis of data obtained during the solar minimum in 1996, they found that the spread F occurrence peaks from May to August, i.e., in the local summer half of the year. However, the observation of plasma bubbles by the CHAMP satellite (Stolle et al. 2006) in 2001–2004 and the measurements of prereversal enhancement of vertical plasma drift (Huang and Hairston 2015) are closer to our findings such that spread F is more frequently observed around equinoxes. Our results concerning the propagation velocities are consistent with previous reports based on optical and GPS total electron content measurements for South America (e.g., Haase et al. 2011) and for Taiwan (Huang 1990; Liu et al. 2011). Our results are based on larger numbers of events and cover the entire year. Pacheco et al. (2011) studied the superrotation and zonal ion drift from the ROCSAT-1 satellite orbiting at an altitude of ~600 km from November 1999 to December 2003, which corresponds to the solar maximum. Their results are consistent with our results in that they observed the largest nighttime eastward drifts in the American sector during the northern winter; similar behavior was shown in the neutral winds. They observed the lowest nighttime eastward drifts from May to August.

In theory, the plasma velocities, or drifts, in the nighttime equatorial F layer should approach the velocities of neutral zonal winds (Kelley 2009). It is therefore useful to compare the observed velocities of OSSs with the velocities of neutral winds obtained by the recent global empirical HWM14 model (Drob et al. 2015). Figure 14a, b presents a comparison between the measured velocities of OSSs and horizontal neutral winds from HWM14 at

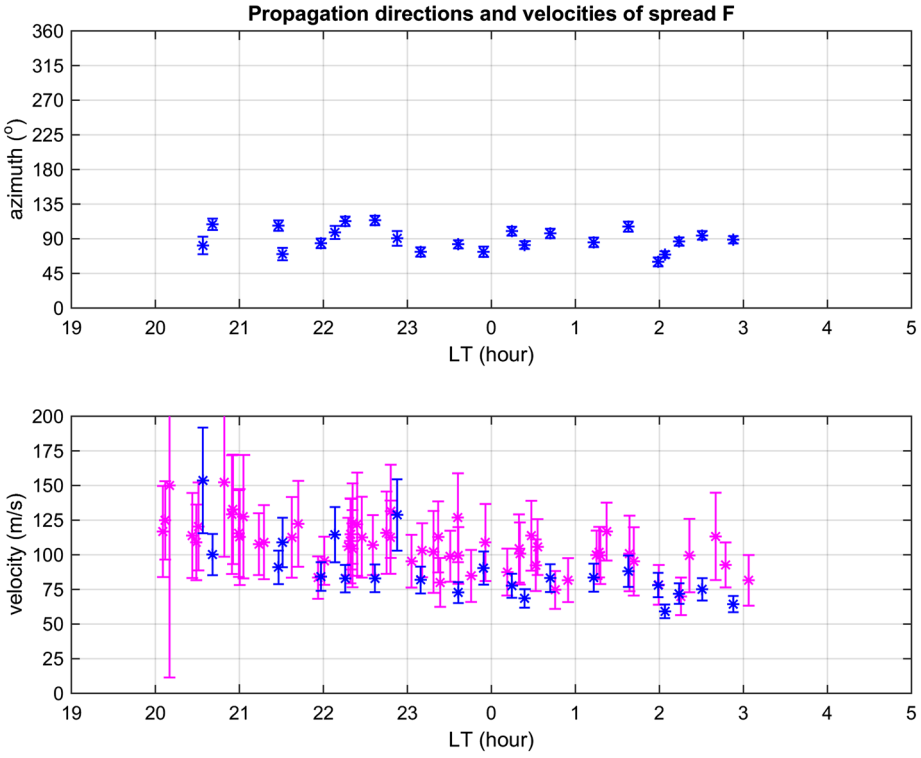

Fig. 11 Azimuths (*top*) and horizontal propagation (*bottom*) velocities of oblique spread structures (OSSs) as a function of daytime for Taiwan in 2014. Values determined by the time delay method are shown in *blue*; and velocities determined by the tilt method are shown in *magenta*

the estimated heights ("Measurements and data analysis" section) and times of observations for Tucumán and Taiwan, respectively. Magenta and blue colors are used for velocities determined by the tilt and time delay methods, respectively. The dashed lines show the velocity coordinates for which the OSS velocities equal the expected neutral wind velocities. Figure 14 shows that the OSS velocities are generally larger than the neutral wind velocities. Obviously, nighttime measurements at the two points are not sufficient for reliable validation of the models; however, they can indicate model limitations. Moreover, the fact that the uncertainties of measured velocities and wind values are relatively large makes the comparison rather qualitative. The fact that the OSS velocities are mostly larger than neutral winds from HWM14 model can be explained by several factors. First, the climatological HWM14 model provides inadequate values of neutral winds, specifically plasma drifts, for spread F conditions. Second, the OSS velocities are measured incorrectly. However, we note that the velocities were determined by two independent methods that gave consistent results within the estimated uncertainties; thus, it is unlikely that both methods would give systematically larger values. In addition, the OSS velocities are consistent with propagation velocities obtained from airglow measurements at 630 nm in Taiwan (Liu et al. 2011). Hence, we consider the first possibility to be the most probable. It is interesting in this respect that the importance of strong neutral winds in the bottomside equatorial ionosphere for the development of ESF was predicted in numerical simulations by Kudeki et al. (2007). However, our measurements were obtained at the low-latitude F2 layer rather than from the equator; thus, they are not fully decisive as the zonal drift of spread F need not be consistent with the "local" neutral wind in the off-equatorial region. Considering the flux-tube-integrated system, the neutral wind over the dip equator or the opposite hemisphere may affect the F-region dynamo. If the bottomside equatorial neutral winds could be at least roughly approximated by the OSS velocities observed at the low latitudes, the fact that we measured larger velocities in Tucumán than in Taiwan could also partially explain the fact that we observed about four times as many events in Tucumán than in those Taiwan (Fig. 10). However, we cannot exclude that other factors such as GW seeding and magnetic field configuration also play important roles. It should be mentioned that the strength and geometry of the geomagnetic field differ between the regions. The strength of the geomagnetic field is lower in Tucumán than in Taiwan. Moreover,

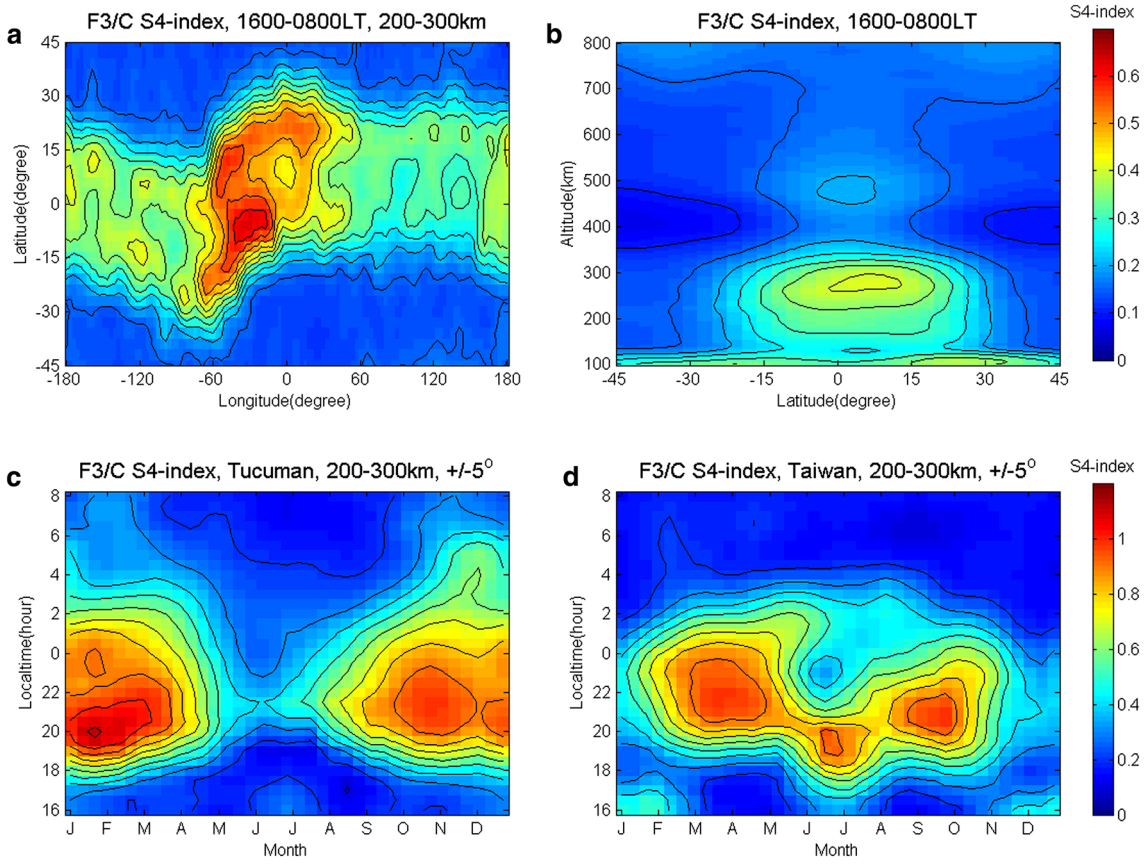

Fig. 12 **a** Global distribution of $S4_{max}$ values for the 200–300 km altitude range. **b** Dependence of $S4_{max}$ on altitude and latitude for the longitude of maximum in Fig. 8a. **c**, **d** $S4_{max}$ values for the 200–300 km altitude range as a function of local time and season over Tucumán and Taiwan, respectively

the magnetic field inclination I is lower in Tucumán, at $I = 27°$, than in Taiwan, at $I = 35°$, even though the distance from the geomagnetic equator is slightly larger by about 200 km for Tucumán than for Taiwan; Tucumán is affected by the South Atlantic magnetic anomaly. Both the weaker magnetic field and more horizontal geometry of the magnetic field could be favorable for spread F initiation. It should be considered that non-migrating tides also produce longitudinal patterns (e.g., Xiong and Luhr 2013) in the EIA. In addition, the EIA can exhibit asymmetry between hemispheres, and the position of the trough can be shifted from the geomagnetic equator (Yue et al. 2015). The exact explanation of mechanisms leading to different occurrence rates and their relative roles requires sophisticated numerical simulations, which is outside the scope of this experimental study.

GW seeding as a potential mechanism for the initiation of ESF and plasma bubble development has been discussed in many experimental and theoretical papers (e.g., Abdu et al. 2009b; Cabrera et al. 2010; Hysell et al. 2014, and references therein). Unfortunately, our observations are under the crest of the EIA rather than at the geomagnetic equator, where the initiation is expected, and the GW seeding in the bottomside ionosphere should be important. Hence, we were unable to draw conclusions from our observations. For completeness, we note only that we usually did not observe significant GW wave activity prior to the OSS events in the Doppler shift spectrograms. We observed noticeable unusual waves that preceded about 10 % of the OSS events, as shown in the example in Fig. 1. The waves propagated roughly eastward in all cases. Their observed propagation velocities obtained by slowness search, which is the method described by Chum et al. (2014), were slightly larger or the same as the propagation velocities of the OSSs. More precisely, they fit the propagation velocities of the OSSs within the estimated uncertainties. This result indicates that their horizontal velocities in the wind frame were very small, at close to zero or on the order of ~10 m s^{-1}, if we assume that OSSs propagate with neutral winds. Therefore, we were not able to distinguish whether we observed real GWs or simply undulations in the vicinity

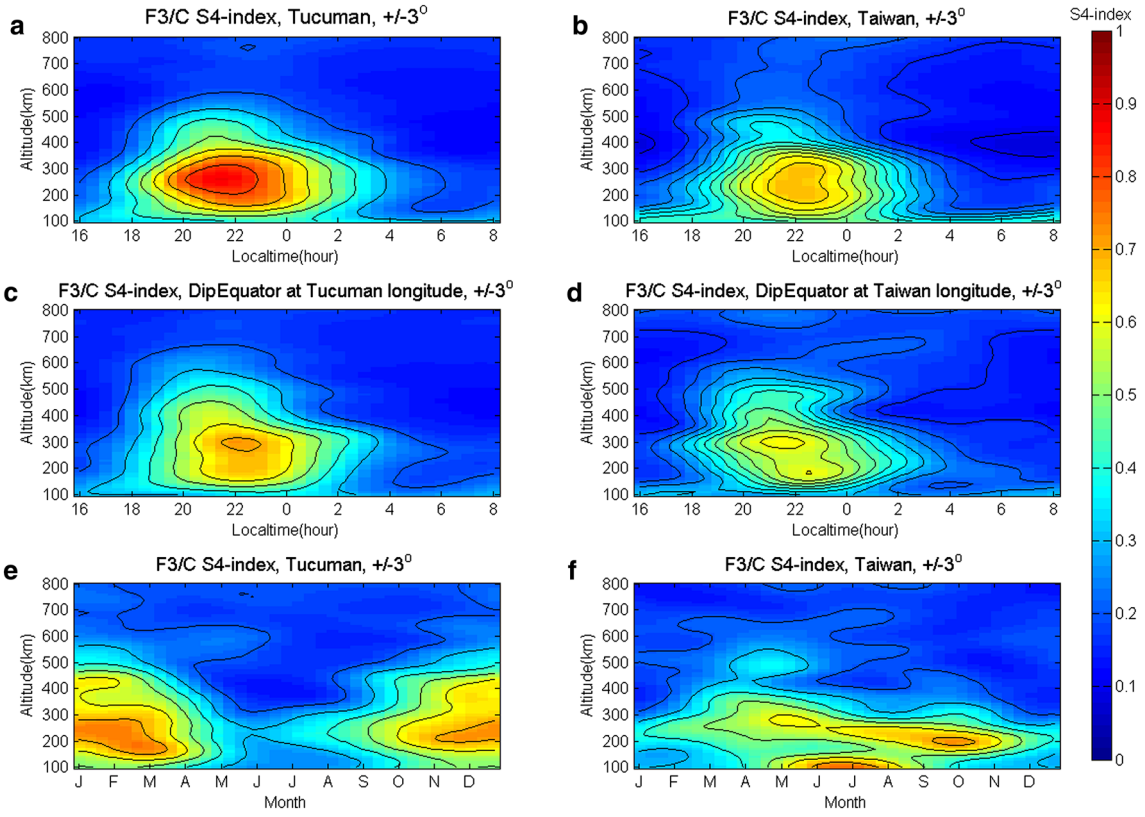

Fig. 13 **a**, **b** $S4_{max}$ values as a function of local time and altitude for Tucumán and Taiwan, respectively. **c**, **d** $S4_{max}$ values as a function of local time and altitude at the geomagnetic equator magnetically conjugated with Tucumán and Taiwan, respectively. **e**, **f** $S4_{max}$ values as a function of season and altitude for Tucumán and Taiwan, respectively

of spread F irregularities that were generated together with spread F. The observations of noticeable wave-like perturbations that preceded about ~10 % of the OSS events can be briefly summarized as follows. (1) If present, the waves occur before the first OSS event at the given night, i.e., relatively soon after sunset, and they sometimes merge with the first OSS events. They have not been observed before the OSS events that occurred late at night. (2) The amplitudes, or Doppler shifts, of waves are usually larger on sounding paths that are closer to the equator (e.g., Fig. 1). We note that the distances between the transmitters are about 100 km; hence, the distances between the reflection points are about 50 km ("Measurements and data analysis" section). (3) It is not possible to accurately determine the velocity and propagation direction for all observations. However, the propagation characteristics of GWs for which the propagation analysis is feasible are similar to propagation of the related OSSs. It should also be noted in this respect that GWs usually do not propagate eastward, particularly in Tucumán (Chum et al. 2014). It is therefore probable that we observed only undulation related to the OSSs rather than real GWs.

It is also interesting to note that we did not observe a systematic decrease in the Doppler shift before the OSSs events, which could indicate uplift of the F layer, particularly that of the reflecting level for the sounding frequency f_0. However, as previously noted, our observations are under the crest of EIA and not under the geomagnetic equator, where the initiation of instability is expected.

Conclusions

Continuous Doppler sounding was applied to study the occurrence rates and propagation velocities of OSSs in Tucumán and Taiwan. The observed OSSs can be related to the equatorial/low-latitude spread F and roughly eastward propagation in both Tucumán and Taiwan. The observed horizontal velocities of the OSSs were in the range of ~70 to ~200 m s^{-1}. The mean velocities over Tucumán, at ~140 m s^{-1}, were higher than those over Taiwan, at ~107 m s^{-1}. In addition, the occurrence rate of

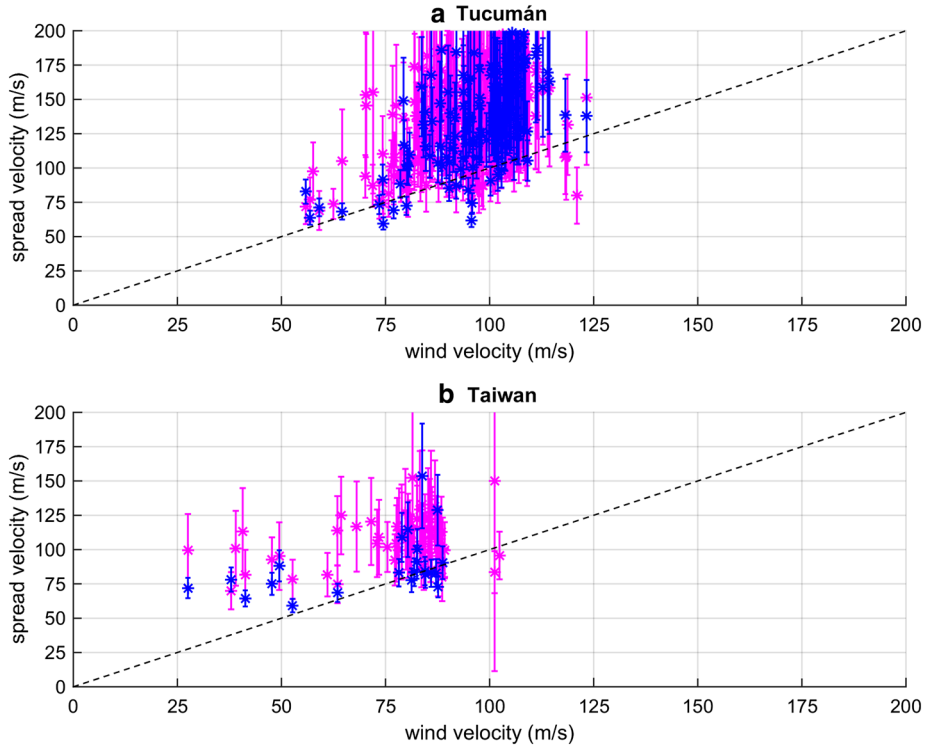

Fig. 14 Comparison of oblique spread structure (OSS) velocities with horizontal neutral winds determined by the HWM14 model at heights and times of observations for **a** Tucumán and **b** Taiwan. Values determined by the time delay method shown in *blue*; velocities determined by the tilt method shown in *magenta*. The *dashed line marks* the spread velocity equal to the HWM14 neutral wind model velocity

the OSS events in Tucumán was about four times higher than that in Taiwan.

It was shown that spread F occurred at the equatorial region at very low latitudes in Jicamarca during the nights of OSS observations in Tucumán and in Sanya during the nights of OSS observations in Taiwan. It was found that spread F usually occurs longer at these equatorial stations.

The GPS signal scintillation data obtained by radio occultation measurements onboard the F3/C satellite are consistent with the occurrences of OSSs in the Doppler data and show a similar seasonal and local time dependence in both Tucumán and Taiwan. The largest values of $S4_{max}$ scintillation index were observed at about the same local times (~20:00 to ~23:00 LT) as the highest velocities and occurrence rates of OSSs observed by Doppler. In addition, global maps of the $S4_{max}$ index and the dependence of $S4_{max}$ on altitude were presented. The main contributions to the GPS signal scintillations, i.e., the highest values of $S4_{max}$, were observed at the altitudes of the F2 layer around the geomagnetic equator in the region of EIA.

The propagation velocities at both locations were usually larger than the horizontal velocities of neutral winds estimated by the HWM14 experimental model. This might indicate that the HWM14 is not suitable enough for determining plasma drifts at the crest of EIA during the spread F conditions, at least over Tucumán and Taiwan.

Authors' contributions

JC wrote most of the paper and performed the analysis of the Doppler measurements. JYL and SPC contributed by examining the F3/C scintillation data and related analysis and the ionosonde data in Taiwan. MAC is responsible for the operation of Doppler sounding in Tucumán and worked with RGE to analyze the ionosonde data in Tucumán. JL helped with the text of the paper, particularly with the introduction and comparison with previous works. DB suggested the comparison with neutral winds. JB, JF, and FH helped with the Doppler shift measurements and data analysis. All authors read and approved the final manuscript.

Author details

[1] Institute of Atmospheric Physics, Bocni II/1401, 14131 Prague 4, Czech Republic. [2] Institute of Space Science, National Central University, Chung-Li 320, Taiwan. [3] Laboratorio de Telecomunicaciones, Facultad de Ciencias Exactas y Tecnología (FACET), Universidad Nacional de Tucumán (UNT), San Miguel deTucumán, Argentina. [4] CIASuR, FRT, Universidad Tecnológica Nacional, San Miguel deTucumán, Argentina. [5] CONICET, Buenos Aires, Argentina.

Acknowledgements

The Doppler data are available at http://datacenter.ufa.cas.cz/under the link to the Spectrogram archive. The IRI-2012, http://omniweb.gsfc.nasa.gov/vitmo/iri2012_vitmo.html, is acknowledged for providing the electron

density profile from which the reflection heights were obtained. The NASA National Space Science Data Center, http://nssdcftp.gsfc.nasa.gov/models/, is acknowledged for providing the source code of the IGRF magnetic field model. The DPS4 portable sounder database is acknowledged for providing ionograms from Jicamarca and Sanya. The support under Grants 15-07281J and P209/12/2440 by the Czech National Foundation, Project M100421201 of the Czech Academy of Sciences, Project MOST104-2923-M-008-002-MY3 Granted to National Central University, Taiwan, and Projects PICT2011-1008 (FONCyT) and PIUNT-UNT 26/E508, Argentina, are acknowledged. J.E. Ise, J.I. Cangemi, and Y. Chen are acknowledged for the maintenance of the Doppler system in Tucumán and Taiwan. V. Truhlik is acknowledged for help with the HWM14 model.

Competing interests

The authors declare that they have no competing interests.

Received: 4 November 2015 Accepted: 29 March 2016
Published online: 08 April 2016

References

Abdu MA, Batista IS, Reinisch BW, De Souza JR, Sobral JHA, Pedersen TR, Medeiros AF, Schuch NJ, De Paula ER, Groves KM (2009a) Conjugate point equatorial experiment (COPEX) campaign in Brazil: electrodynamics highlights on spread F development conditions and day-to-day variability. J Geophys Res 114:A04308. doi:10.1029/2008JA013749

Abdu MA, Kherani EA, Batista IS, De Paula ER, Fritts DC, Sobra JHA (2009b) Gravity wave initiation of equatorial spread F/plasma bubble irregularities based on observational data from the SpreadFEx campaign. Ann Geophys 27:2607–2622

Alfonsi L, Spogli L, Pezzopane M, Romano V, Zuccheretti E, De Franceschi G, Cabrera MA, Ezquer RG (2013) Comparative analysis of spread-F signature and GPS scintillation occurrences at Tucumán, Argentina. J Geophys Res Space Phys 118:4483–4502. doi:10.1002/jgra.50378

Arras C, Wickert J, Beyerle G, Heise S, Schmidt T, Jacobi C (2008) A global climatology of ionospheric irregularities derived from GPS radio occultation. Geophys Res Lett 35:L14809. doi:10.1029/2008GL034158

Bhattacharyya A, Burke WJ (2000) A transmission line analogy for the development of equatorial ionospheric bubbles. J Geophys Res 105:24941–24950

Cabrera MA, Pezzopane M, Zuccheretti E, Ezquer RG (2010) Satellite traces, range spread-F occurrence, and gravity wave propagation at the southern anomaly crest. Ann Geophys 28:1133–1140. doi:10.5194/angeo-28-1133-2010

Chen WS, Lee CC, Liu JY, Chu FD, Reinisch BW (2006) Digisonde spread F and GPS phase fluctuations in the equatorial ionosphere during solar maximum. J Geophys Res 111:A12305. doi:10.1029/2006JA011688

Chum J, Hruska F, Zednik J, Lastovicka J (2012) Ionospheric disturbances (infrasound waves) over the Czech Republic excited by the 2011 Tohoku earthquake. J Geophys Res 117:A08319. doi:10.1029/2012JA017767

Chum J, Bonomi FAM, Fišer J, Cabrera MA, Ezquer RG, Burešová D, Laštovička J, Baše J, Hruška F, Molina MG, Ise JE, Cangemi JI, Šindelářová T (2014) Propagation of gravity waves and spread F in the low-latitude ionosphere over Tucumán, Argentina, by continuous Doppler sounding: first results. J Geophys Res Space Phys 119:6954–6965. doi:10.1002/2014JA020184

Davies K, Baker DM (1966) On frequency variations of ionospherically propagated HF radio signals. Radio Sci 1:545–556

Davies K, Watts J, Zacharisen D (1962) A study of F2-layer effects as observed with a Doppler technique. J Geophys Res 67:2. doi:10.1029/JZ067i002p00601

Drob DP, Emmert JT, Meriwether JW, Makela JJ, Doornbos E, Conde M, Hernandez G, Noto J, Zawdie KA, McDonald SE, Huba JD, Klenzing JH (2015) An update to the horizontal wind model (HWM): the quiet time thermosphere. Earth Space Sci 2:301–319. doi:10.1002/2014EA000089

England SL, Immel TJ (2012) An empirical model of the drift velocity of equatorial plasma depletions. J Geophys Res 117:A12308. doi:10.1029/2012JA018091

Ezquer RG, Kintner PM, Cabrera MA, Radicella SM, Forte B (2003) Scintillations observed at Tucuman as observed from GPS signals. First results. Adv Space Res 31(3):741–747

Fejer BG, Scherliess L, De Paula ER (1999) Effects of the vertical plasma drift velocity on the generation and evolution of equatorial spread F. J Geophys Res 104:19859–19870. doi:10.1029/1999JA900271

Fejer BG, Souza JR, Santos AS, Costa Pereira AE (2005) Climatology of F region zonal plasma drifts over Jicamarca. J Geophys Res 110:A12310. doi:10.1029/2005JA011324

Haase JS, Dautermann T, Taylor MJ, Chapagain N, Calais E, Pautet D (2011) Propagation of plasma bubbles observed in Brazil from GPS and airglow data. Adv Space Res 47(10):1758–1776. doi:10.1016/j.asr.2010.09.025

Hartmann GA, Pacca IG (2009) Time evolution of the South Atlantic Magnetic Anomaly. An Acad Bras Cienc 81(2):243–255. ISSN 0001-3765

Huang Y-N (1990) Drift motion of ionospheric bubbles at the equatorial anomaly crest region. J Geophys Res 95(A4):4297–4301

Huang C-S, Hairston MR (2015) The postsunset vertical plasma drift and its effects on the generation of equatorial plasma bubbles observed by the C/NOFS satellite. J Geophys Res Space Phys 120:2263–2275. doi:10.1002/2014JA020735

Huang CY, Burke WJ, Machuzak JS, Gentile LC, Sultan P (2001) DMSP observations of equatorial plasma bubbles in the topside ionosphere near solar maximum. J Geophys Res 106:8131–8142

Hysell DL, Jafari R, Fritts DC, Laughman B (2014) Gravity wave effects on postsunset equatorial F-region stability. J Geophys Res Space Phys 119:5847–5860. doi:10.1002/2014JA019990

Kelley MC (2009) The Earth's ionosphere, plasma physics and electrodynamics, 2nd edn. Elsevier, Amsterdam

Keskinen MJ, Ossakow SL, Basu S, Sultan PJ (1998) Magnetic flux-tube-integrated evolution of equatorial ionospheric plasma bubbles. J Geophys Res 103:3957–3967

Kil H, Kintner PM, de Paula ER, Kantor IJ (2002) Latitudinal variations of scintillation activity and zonal plasma drifts in South America. Radio Sci. doi:10.1029/2001RS002468

Kudeki E, Akgiray A, Milla M, Chau JL, Hysell DL (2007) Equatorial spread-F initiation: post-sunset vortex, thermospheric winds, gravity waves. J Atmos Sol Terr Phys 69:2416–2427. doi:10.1016/j.jastp.2007.04.012

Lee C-C, Chen WS, Chu FD (2013) Observation of F region irregularities near a northern equatorial anomaly crest during solar minimum using ionosonde, GPS receiver, and satellites. J Geophys Res Space 118:3613–3621. doi:10.1002/jgra.50350

Liu JY, Rajesh PK, Lee IT, Chow TC (2011) Airglow observations over the equatorial ionization anomaly zone in Taiwan. Ann Geophys 29:749–757

Luhr H, Rother M, Maus S, Mai W, Cooke D (2003) The diamagnetic effect of the equatorial Appleton anomaly: its characteristics and impact on geomagnetic field modeling. Geophys Res Lett 30(17):1906. doi:10.1029/2003GL017407

Martinis C, Eccles JV, Baumgardner J, Manzano J, Mendillo M (2003) Latitude dependence of zonal plasma drifts obtained from dual-site airglow observations. J Geophys Res 108(A3):1129. doi:10.1029/2002JA009462

McNamara LF, Retterer JM, Abdu MA, Batista IS, Reinisch BW (2008) F2 Peak parameters, drifts and spread F derived from digisonde ionograms for the COPEX campaign in Brazil. J Atmos Sol Terr Phys 70:1144–1158

Muella MTAH, de Paula ER, Kantor IJ, Rezende LFC, Smorigo PF (2009) Occurrence and zonal drifts of small-scale ionospheric irregularities over an equatorial station during solar maximum—magnetic quiet and disturbed conditions. Adv Space Res 43:1957–1973

Pacheco EE, Heelis RA, Su S-Y (2011) Superrotation of the ionosphere and quiet time zonal ion drifts at low and middle latitudes observed by Republic of China Satellite-1 (ROCSAT-1). J Geophys Res 116:A11329. doi:10.1029/2011JA016786

Park J, Min KW, Kim VP, Kil H, Lee J-J, Kim H-J, Lee E, Lee DY (2005) Global distribution of equatorial plasma bubbles in the premidnight sector during solar maximum as observed by KOMPSAT-1 and Defense meteorological Satellite Program F15. J Geophys Res 110:A07308. doi:10.1029/2004JA010817

Shi JK, Wang GJ, Reinisch BW, Shang SP, Wang X, Zherebotsov G, Potekhin A (2011) Relationship between strong range spread F and ionospheric scintillations observed in Hainan from 2003 to 2007. J Geophys Res 116:A08306. doi:10.1029/2011JA016806

Smith JM, Rodrigues FS, de Paula ER (2015) Radar and satellite investigations of equatorial evening vertical drifts and spread F. Ann Geophys 33:1403–1412. doi:10.5194/angeo-33-1403-2015

Stolle C, Luhr H, Rother M, Balasis G (2006) Magnetic signatures of equatorial spread F as observed by the CHAMP satellite. J Geophys Res 111:A02304. doi:10.1029/2005JA011184

Sultan PJ (1996) Linear theory and modeling of the Rayleigh–Taylor instability leading to the occurrence of equatorial spread F. J Geophys Res 101:26875–26891

Terra PM, Sobral JHA, Abdu MA, Souza JR, Takahashi H (2004) Plasma bubble zonal velocity variations with solar activity in the Brazilian region. Ann Geophys 22:3123–3128

Xiong C, Lühr H (2013) Non-migrating tidal signatures in the magnitude and the inter-hemispheric asymmetry of the equatorial ionization anomaly. Ann Geophys 31:1115–1130

Yue X, Schreiner WS, Kuo Y-H, Lei J (2015) Ionosphere equatorial ionization anomaly observed by GPS radio occultations during 2006-2014. J Atmos Sol Terr Phys 129:30–40. doi:10.1016/j.jastp.2015.04.004

Zhang Y, Wan W, Li G, Liu L, Hu L, Ning B (2015) A comparative study of GPS ionospheric scintillations and ionogram spread F over Sanya. Ann Geophys 33:1421–1430. doi:10.5194/angeo-33-1421-2015